International Journal of Thermophysics, Vol. 23, No. 6, November 2002 (© 2002)

NEMD Simulations of Viscosity and Viscosity Index for Lubricant-Size Model Molecules

Y. Yang,[1] T. A. Pakkanen,[2] and R. L. Rowley[1, 3]

Received April 8, 2002

Synthetic lubricant research can be facilitated with nonequilibrium molecular dynamics simulations (NEMD) of viscosity and viscosity index (*VI*). While previously reported simulations using united atom (UA) models for intermolecular interactions have generally under-predicted the viscosity of lubricant-size alkanes, *VI* values, trends with respect to structure, and viscosity pressure coefficients obtained from simulations are generally accurate, suggesting that simulations of UA models can be used for screening candidate fluids. This requires some reliance on the expected accuracy of the method as established by application to a wide variety of model fluids. We report here the results of NEMD simulations on UA models for 2,2,4,4,6,8,8-heptamethylnonane (HMN) and 11-*n*-amylheneicosane (NAH). HMN represents a molecule with significant branching, dominated with tertiary carbons; NAH represents a fluid with a single large aliphatic branch off of a long aliphatic chain, and a molecule for which there is some interest as a lubricant component. Additionally, we test here a new parameterization of UA potentials for $-CH_X$ groups. *VI* results from simulations using the new parameterization are in excellent agreement with experiment. Viscosity results are significantly better with the new parameterization, but the UA model still tends to underestimate the viscosity of larger, lubricant-size molecules.

KEY WORDS: molecular dynamics; nonequilibrium molecular dynamics; lubricants; viscosity; viscosity index.

1. INTRODUCTION

Viscosity and viscosity index (*VI*) are key design properties for development and selection of synthetic lubricants. *VI* characterizes the temperature

[1] Department of Chemical Engineering, 350CB, Brigham Young University, Provo, Utah 84602, U.S.A.
[2] Department of Chemistry, University of Joensuu, Joensuu, Finland.
[3] To whom correspondence should be addressed. E-mail: rowley@byu.edu

0195-928X/02/1100-1441/0 © 2002 Plenum Publishing Corporation

dependence of the lubricant's kinematic viscosity: the higher the value of *VI*, the less effect temperature has on the viscosity. Originally, *VI* was calculated by comparing the kinematic viscosity of the lubricant at 311 K and 372 K to reference values for a good and a poor lubricant arbitrarily assigned values of 100 and 0, respectively [1]. The ASTM standard [2] uses a later definition of *VI* [3],

$$VI = 3.63(60 - 10^{n}) \qquad \text{where} \quad n = \frac{\log \nu_1 - \log k}{\log \nu_2}, \tag{1}$$

to accommodate a wider range of viscosity. Here ν_1 is the kinematic viscosity in square millimeter per second (mm^2/s or cSt) at 311 K, ν_2 is the kinematic viscosity in mm^2/s at 372 K (and presumably 0.1 MPa), and $k = 2.714$. Another measure of a lubricant's temperature independence is the viscosity number (*VN*), which is calculated by using the kinematic viscosities (in mm^2/s) at 313 K and 373 K to obtain the coefficients *A* and *B* in the equation

$$\log[\log(\nu + 0.7)] = A + B \log(T). \tag{2}$$

The value of *B* thus obtained is used in

$$VN = \left(1 + \frac{3.55 + B}{3.55}\right) \times 100 \tag{3}$$

to obtain *VN*. *VN* values obtained in this manner correlate well with *VI* but permit a wider range in temperature.

Development of synthetic lubricants, with viscosity and *VI* tuned to the intended application, is expected to involve testing of a very large number of potential molecules and their mixtures. Chemical synthesis of candidate fluids and measurement of viscosity at a variety of conditions (e.g., engine operating temperatures) makes an experimental approach to this task prohibitively expensive. Molecular simulation of fluid viscosity and *VI* offers a method for both screening potential lubricants in order to minimize experimental work and guiding the search for the structural characteristics of the molecule that produce the desired macroscopic properties. Simulation of viscosity using nonequilibrium molecular dynamics (NEMD) has been well established since its inception over two decades ago, and numerous studies using Gaussian mechanics [4–6] have refined the methodology. Early studies focused on model fluids for linear alkanes, e.g. [7, 8], but more recent studies have extended the method to branched alkanes, e.g. [9–12], molecules containing polar groups [13, 14], mixtures

[15], and most recently to branched alkanes of molecular weight sufficiently high to be considered potential lubricants [16–19].

Differences between experimental and simulated viscosities are primarily attributable to either (1) inadequacies in the intermolecular potential model or (2) uncertainties in the low-shear viscosity ascertained from nonequilibrium simulations which necessarily apply shear rates several orders of magnitude higher than those used in experiments. The latter difficulty is resolved by extrapolation to low shear rates [7, 9, 12], fitting shear-dependent data to a rheological model [18], or by performing longer simulations at lower shear rates until one can identify a change in rheology from shear thinning (at the higher shear rates) to a Newtonian plateau at lower shear rates [17, 19]. Model efficacy, on the other hand, remains the main avenue for improvement of results, and it is receiving a great deal of attention and research effort. However, because of the computational times involved, united-atom (UA) models in which $-CH_X$ groups are modeled as single interacting sites (as opposed to individual sites at each atomic center) have been used almost exclusively for simulations of moderately-sized molecules.

While future improved intermolecular models are highly likely to increase the accuracy of viscosities obtained from simulations, potentially leading to simulation as a standard for accurate prediction of viscosities, the UA model results to date have provided sufficient accuracy to be useful for screening purposes and for illuminating structural trends in viscosity and *VI*. Indeed, even as better potential models become available, this utility of UA models for initial screening of many potential fluids will likely remain, owing to the significant savings in CPU time afforded by the model. This use of NEMD simulations to screen potential lubricants, however, requires confidence in the consistency of the predictions and knowledge of the expected accuracy of the simulation results for the underlying model fluid.

This knowledge and understanding must be built on experience and results from simulations on a variety of model fluids. For example, Moore et al. [16] reported excellent results for both the viscosity and *VI* of squalane (C30) using an UA model. Simulated kinematic viscosities were within about 6% of experimental values. Agreement between experimental and simulated *VI* values was even better: values were 115 from simulation and 116 from experiment. However, simulation results have not been as sanguine for other UA model fluids. Table I shows a comparison of simulated viscosities and *VI* values compared to experimental values. As can be seen, NEMD simulations using UA models, with Lennard-Jones (LJ) parameters regressed from equilibrium properties, typically underestimate the viscosity, often by a factor of two. As several of the studies

shown in Table I use the most recent equilibrium alkane potential parameters [21], it is evident that further optimization of parameters from equilibrium properties will not resolve the problem of low simulated values. On the other hand, simulated values of *VI* or *VN* are seen to be in pretty good agreement with experimental values. Trends in viscosity with respect to temperature, pressure, and molecular structure generally agree with experiment.

In this work, we use NEMD simulations to determine the viscosity and *VI* for 2,2,4,4,6,8,8-heptamethylnonane (HMN, C16) and 11-*n*-amylheneicosane (NAH, C26). The purpose of this work is to provide additional information on the performance of UA models in simulating viscosity and *VI* for different types of molecules large enough to qualify as potential lubricants. HMN represents a molecule with significant branching, dominated with tertiary carbons. NAH represents a fluid with a single large aliphatic branch off of a long aliphatic chain, and a molecule for

Table I. Comparison of Simulated and Experimental Kinematic Viscosity (ν) or Dynamic Viscosity (η) and *VI* or *VN* Values for Fluids of Molecular Weight in the Range Appropriate for Potential Lubricants

Molecule	Property	Sim.	Exp.	% Diff.	Ref.
Squalane (C30)	ν, 311 K	19.7 $mm^2 \cdot s^{-1}$	20.9 $mm^2 \cdot s^{-1}$	−6	16
	ν, 372 K	4.06 $mm^2 \cdot s^{-1}$	4.2 $mm^2 \cdot s^{-1}$	−3	
	VI	115	116	−1	
n-C30	ν, 311 K	2.3 $mm^2 \cdot s^{-1}$	4.4 $mm^2 \cdot s^{-1}$	−48	19
9-*n*-Octyldocosane	ν, 311 K	7.3 $mm^2 \cdot s^{-1}$	14.4 $mm^2 \cdot s^{-1}$	−49	19
(C30)	ν, 372 K	2.3 $mm^2 \cdot s^{-1}$	3.6 $mm^2 \cdot s^{-1}$	−57	
	VI	153	143	6.5	
Squalane (C30)	ν, 311 K	18.2 $mm^2 \cdot s^{-1}$	20.9 $mm^2 \cdot s^{-1}$	−13	19
	ν, 372 K	3.8 $mm^2 \cdot s^{-1}$	4.2 $mm^2 \cdot s^{-1}$	−10	
	VI	103	116	−11	
n-C16	η, 298 K	1.57 mPa·s	3.09 mPa·s	−49	11
n-C28	η, 373 K	1.62 mPa·s	2.88 mPa·s	−44	11
9-Octylheptadecane	η, 372 K, 0.1 MPa	1.36 mPa·s	1.86 mPa·s	−27	20
(C25)	η, 372 K, 0.7 GPa	87 mPa·s	186 mPa·s	−53	
	η , 372 K, 0.8 GPa	165 mPa·s	358 mPa·s	−54	
	η, 372 K, 1.0 GPa	270 mPa·s	621 mPa·s	−56	
n-C18	ν, 313 K	2.5 $mm^2 \cdot s^{-1}$	3.9 $mm^2 \cdot s^{-1}$	−36	18
	ν, 373 K	1.2 $mm^2 \cdot s^{-1}$	1.6 $mm^2 \cdot s^{-1}$	−33	
	VN	101	103	−1	

which there is some interest as a lubricant component. Additionally, we test here a new parameterization of UA LJ potentials for $-CH_X$ groups which may be useful in viscosity simulations.

2. SIMULATION DETAILS

Structural models for HMN and NAH were taken from the optimized geometry obtained from Gaussian 98 [22] HF/6-311G *ab initio* calculations. Gaussian mechanics were used in the NEMD simulations to fix bond lengths and angles at the optimum values obtained from the *ab initio* calculations. Values for these structural properties are given in Table II; Fig. 1 depicts the models and identifies the labels used in Table II. Although bond lengths and bond angles were frozen in the NEMD simulations, torsional potentials were included using the equations and parameters developed by Mondello and Grest [23].

An UA description of intermolecular interactions was used in which the methyl, methylene, and methyne groups were each treated as individual LJ interaction sites centered on the carbon nucleus. Pairwise additivity was assumed between all of the sites, including intramolecular interactions between sites separated by three or more bonds. Two different sets of LJ parameters were used in the HMN simulations. The first set, obtained by Jorgensen et al. [24] by optimizing the parameters to agree with liquid density and heat of vaporization data, is called Model 0, and values are listed in Table III. The second set retains the ε values given in Table III, but replaces the σ values with those calculated from the correlation proposed by Yang [25],

$$\begin{bmatrix} \sigma = 0.4090 \text{ nm} & (\text{for } -CH_3 \text{ if connected to } -CH_2 \text{ or } >CH \text{ group}) \\ \sigma = 0.3800 + Kn_H \text{ nm} & (\text{for all other } -CH_X \text{ groups}) \end{bmatrix}, \tag{4}$$

where n_H is the number of hydrogen atoms bonded to the carbon center, and K is a constant which we define later in conjunction with different models. This latter correlation was proposed as a way to systematically account for the additional drag of the hydrogen atoms under shear. The difference between the σ values for the two sets is very small, as shown in Table III, but it has a significant effect upon simulated viscosity.

NEMD simulations under planar Couette flow were performed using the SLLOD equations of motion [26] with Lees–Edwards boundary conditions and a Gaussian thermostat applied to molecular centers of mass. Bond lengths and angles were fixed using Gaussian mechanics [27] applied to bonded sites and next-nearest neighbors, respectively. As in our previous

Table II. Model Bond Lengths and Angles for HMN and NAH Obtained from Geometry Optimization

HMN bond distances (nm)					
1–2	0.15560	2–3	0.15496	2–4	0.15527
2–5	0.15691	5–6	0.15720	6–7	0.15505
6–8	0.15496	6–9	0.15685	9–10	0.15667
10–11	0.15495	10–12	0.15613	12–13	0.15645
13–14	0.15534	13–15	0.15505	13–16	0.15495
HMN bond angles (degrees)					
1–2–3	107.74	1–2–4	107.24	3–2–4	109.23
3–2–5	114.32	1–2–5	105.70	5–6–7	110.97
2–5–6	124.24	5–6–8	113.11	7–6–8	109.39
7–6–9	109.98	5–6–9	104.25	6–9–10	118.09
9–10–11	108.27	11–10–12	111.85	9–10–12	110.55
10–12–13	119.11	12–13–15	111.14	12–13–14	106.90
14–13–15	108.31	14–13–16	108.26	12–13–16	113.22
NAH bond distances (nm)					
1–2	0.15295	2–3	0.15313	3–4	0.15310
4–5	0.15312	5–6	0.15312	6–7	0.15312
7–8	0.15311	8–9	0.15321	9–10	0.15321
10–11	0.15419	11–12	0.15419	12–13	0.15321
13–14	0.15321	14–15	0.15311	15–16	0.15312
16–17	0.15312	17–18	0.15312	18–19	0.15310
19–20	0.15313	20–21	0.15295	11–22	0.15440
22–23	0.15331	23–24	0.15323	24–25	0.15313
25–26	0.15295				
NAH bond angles (degrees)					
1–2–3	113.1359	2–3–4	113.4420	3–4–5	113.4025
4–5–6	113.4012	5–6–7	113.3986	6–7–8	113.3974
7–8–9	113.3908	8–9–10	112.8236	9–10–11	115.4803
10–11–12	109.5261	11–12–13	115.4799	12–13–14	112.8234
13–14–15	113.3910	14–15–16	113.3974	15–16–17	113.3986
16–17–18	113.4012	17–18–19	113.4025	18–19–20	113.4420
19–20–21	113.1359	10–11–22	113.5781	12–11–22	113.5795
11–22–23	116.3392	22–23–24	112.5536	23–24–25	113.4275
24–25–26	113.1428				

work, a fourth-order-correct predictor-corrector numerical integrator was used to advance the simulation forward in time. The time step size was chosen so that the root-mean-squared local displacement of molecules was 0.4 pm per time step, corresponding to approximately 2.5 fs, and simulations ranged from 150,000 to 5,000,000 time steps in duration beyond

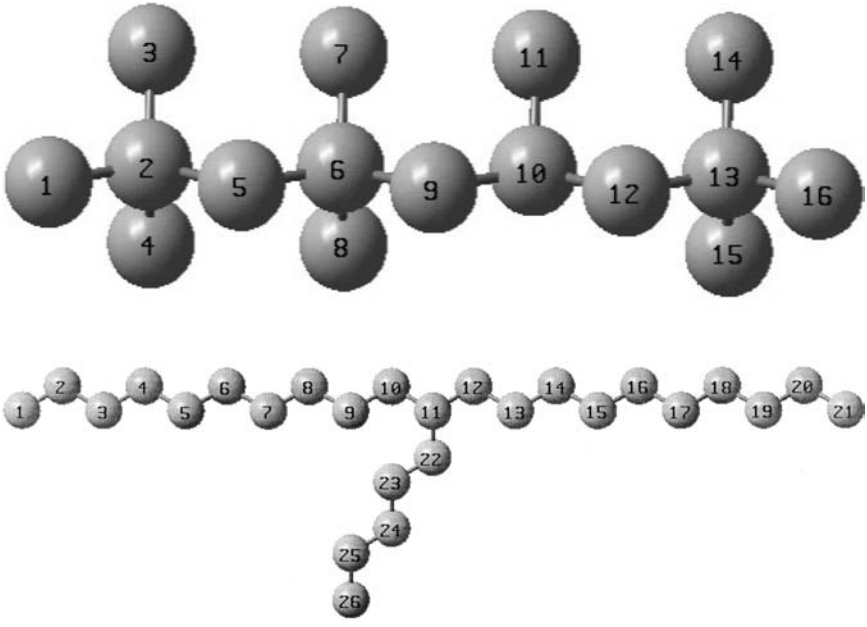

Fig. 1. UA models for HMN (top) and NAH (bottom) identifying the numbering used in Table II.

equilibration, depending upon the applied shear rate. Equilibration consisted of a gradual increase in the density, or decrease in simulation box size, from an initial lattice configuration at low density. Once the density was equivalent to the experimental liquid density, the box size was fixed, the shear was turned on, and NVT simulations were continued for 10,000 additional time steps to equilibrate the system before collecting data.

Table III. Intermolecular LJ Site-Site Parameters

Site	ε^a/k (K)	σ^a (nm)	σ^b (nm)
$-CH_X-CH_3$	88.122	0.3905	0.4090
$-CH_3$	88.122	0.3960	0.4139
$-CH_2-$	59.419	0.3905	0.4026
>CH–	40.284	0.3850	0.3913
>C<	25.178	0.3800	0.3800

[a] Jorgensen et al., 1984 [24].
[b] Eq. (4), Model 1.

The repulsive portion of the LJ potential (r^{-12}) was truncated at $r = 3.0$ nm, and long-range corrections, though generally insignificant, were treated in the standard way. The attractive part of the LJ potential (r^{-6}) was handled using the Ewald sum method as was done previously [13], even though there are no partial charges in the model molecules used in this study. Simulations were performed at several shear rates between 2 and 225 ns^{-1} at each temperature and density to identify the shear-thinning region and the Newtonian plateau at low shear rates. Additional simulations in the Newtonian plateau region (generally between 2 and 6 ns^{-1}) were then performed to provide additional low-shear values in the region where the data are most noisy. The value of the viscosity for comparison to experiment was obtained by a weighted average of the values obtained in the plateau region.

3. RESULTS

Simulations for HMN were performed at three different temperatures and three different densities (corresponding to different pressures) using the two different formulations for the LJ σ values. As mentioned above, simulations were performed at several shear rates in order to distinguish the

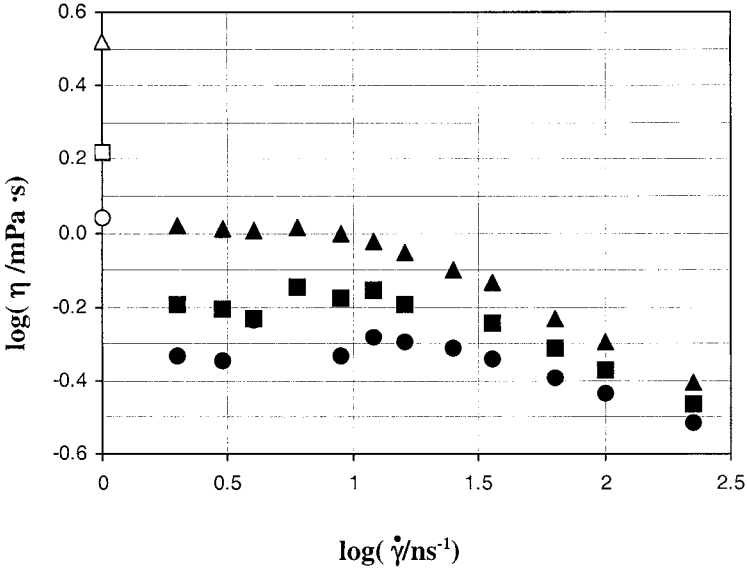

Fig. 2. Shear rate dependence of simulated HMN viscosities at 0.1 MPa and 298 K (▲), 333 K (■), and 363 K (●) using Model 0; experimental values are shown as corresponding open symbols.

Newtonian plateau from the shear thinning region. An example of the results for the three isotherms at 0.1 MPa is shown for HMN as Fig. 2. The two different rheological regions are distinguishable from the simulated results, although viscosities at lower shear rates become less certain. Longer simulation times were employed at the lower shear rates to partially compensate for this decay in signal-to-noise ratio. The results shown in Fig. 2 were obtained using the Jorgensen et al. [24] σ values derived from equilibrium properties, and they are labeled hereafter as Model 0. Consistent with what others have reported (see Table I), simulated viscosities obtained using UA models with parameters regressed from equilibrium data are significantly lower than experimental values at the same conditions.

The sensitivity of the results to the size of the $-CH_X$ group can be seen in Fig. 3, in which simulations in the plateau region were repeated using Eq. (4) with $K = 0.0106$ nm (Model 1) and $K = 0.0119$ nm (Model 2). Model 1 represents about a 4% increase in σ for $-CH_3$ groups attached to a tertiary carbon atom relative to Model 0; Model 2 represents about a 5% increase. As can be observed in Fig. 3, a small change in the LJ size

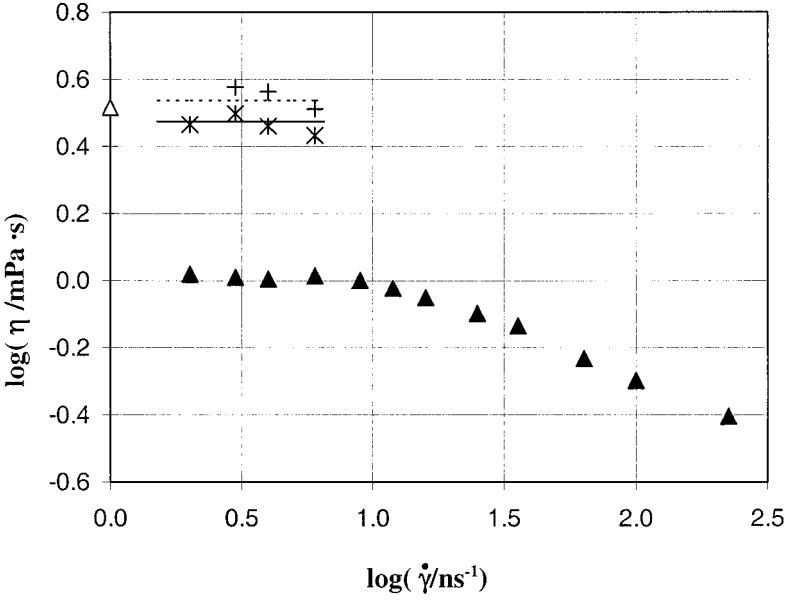

Fig. 3. Comparison of HMN simulated viscosities in the Newtonian plateau region for Model 0 (▲), Model 1 (∗), and Model 2 (+). The experimental value at these conditions, 298 K and 0.1 MPa, is also shown (△) as are the average values obtained at low shear (horizontal lines).

Table IV. Simulated Viscosities for HMN for Various σ Models

P (MPa)	T (K)	ρ (kmol·m^{-3})[a]	η_{exp} (mPa·s)[a]	η (mPa·s) Model 0	η (mPa·s) Model 1	η (mPa·s) Model 2
0.1	298	3.437	3.30	1.03 (−69%)	2.97 (−10%)	3.45 (4%)
	333	3.334	1.66	0.66 (−60%)	1.54 (−7%)	1.83 (10%)
	363	3.247	1.09	0.51 (−53%)	0.95 (−13%)	1.18 (8%)
20	298	3.494	4.67	1.35 (−71%)	4.06 (−13%)	–
	333	3.404	2.29	0.86 (−62%)	2.09 (−9%)	2.52 (10%)
	363	3.326	1.43	0.66 (−54%)	1.26 (−12%)	1.59 (11%)
40	298	3.542	6.60	1.57 (−76%)	6.01 (−9%)	–
	333	3.460	3.10	1.06 (−65%)	2.59 (−14%)	3.54 (18%)
	363	3.389	1.89	0.80 (−58%)	1.70 (−10%)	2.21 (17%)

[a] Ref. 29.

parameter significantly increased the simulated viscosity obtained in the Newtonian plateau region.

The low-shear results for all nine combinations of temperatures and pressures are given in Table IV. Again Model 0 results are substantially too low, generally by a factor of two. Model 1 and Model 2 tend to bracket the experimental values and seem to produce consistent results relative to the experimental values at all conditions.

The rather constant difference between simulated and experimental values as a function of pressure indicates that the pressure coefficient of the viscosity is reliably predicted. This is consistent with the findings of others [20, 28] for different alkanes. Similarly, the consistency of the difference between experimental and simulated viscosities as a function of temperature suggests reliability of the simulations in predicting *VI* or *VN*. This is also confirmed by plotting the kinematic viscosity as a function of inverse temperature as in Fig. 4. While the slope obtained from simulations with Model 0 is somewhat different than experiment, the slopes obtained with Models 1 and 2 agree very well with experiment. Using the linear relationship between $\log(\nu)$ and T^{-1} observed in Fig. 4, the kinematic viscosities can be evaluated at 311 K and 372 K for use in Eq. (1). The resultant *VI* values are shown in Table V. As has been suggested by previous studies, the kinematic viscosity for HMN is predicted accurately by the new UA models. The value obtained from Model 0 is unacceptably poor

Using an average of Model 1 and Model 2 ($K = 0.0112$ nm) in conjunction with Eq. (4), we simulated also the viscosity of NAH at two different temperatures as a function of shear rate. The results are shown in Fig. 5. Again, the Newtonian plateau region was evident from the plot, and

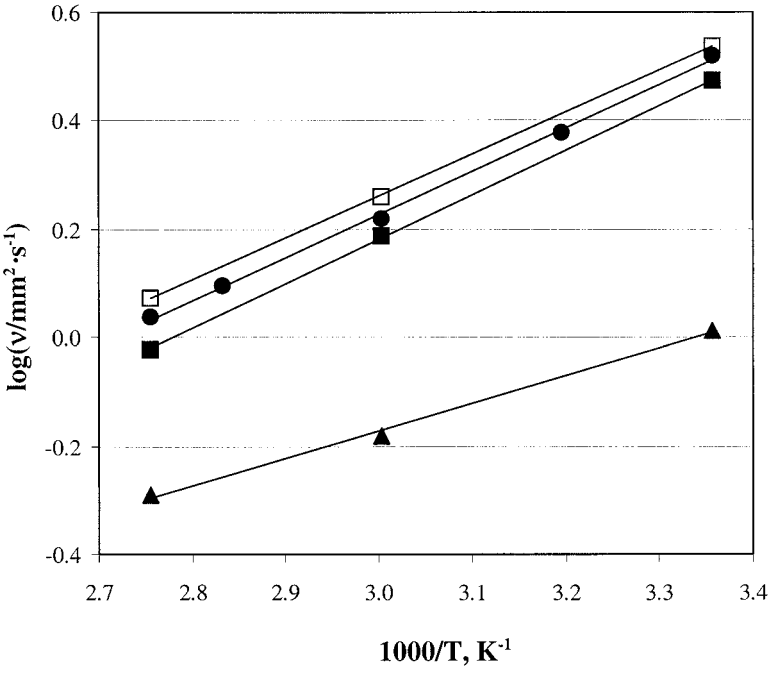

Fig. 4. Temperature dependence of log(v) for HMN from experiment (●), from simulations with Model 0 (▲), Model 1 (■), and Model 2 (□).

the zero-shear value was taken as the average of the simulated values in this region with each point weighted in the average by the inverse of the standard deviation as obtained from block averages (shown as error bars in Fig. 5). The low-shear results and the *VI* value calculated from the results using Eq. (1) are listed in Table VI. Even with the σ value adjusted to the HMN results, the NAH simulated viscosities are low compared to the experimental values. The *VI* value, however, is in reasonably good agreement with the reported experimental value [30].

Table V. Comparison of Simulated HMN *VI* Values

Exp	192
Model 0	9
Model 1	182
Model 2	195

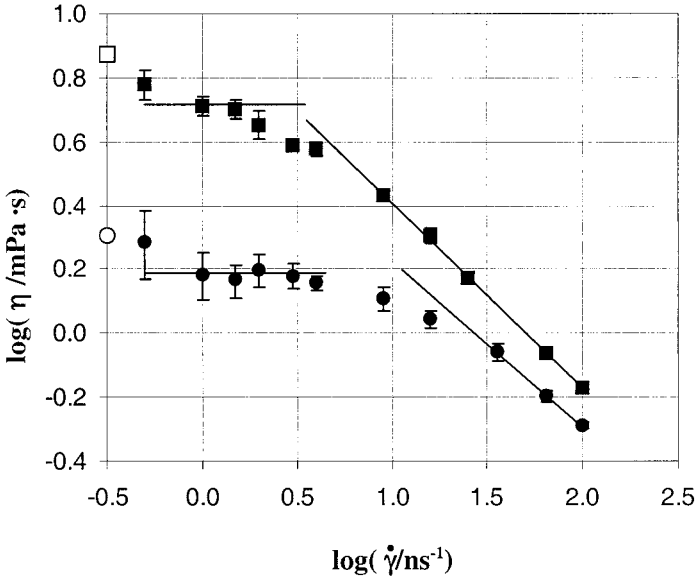

Fig. 5. Shear rate dependence of simulated NAH viscosities at 0.1 MPa and 311 K (■) and 373 K (●) using the average model ($K = 0.0112$ nm); experimental values are shown as corresponding open symbols.

4. CONCLUSIONS

We have performed NEMD simulations on UA models representing HMN and NAH. The Newtonian plateau can be found from the shear-rate dependent results of the simulations, but the resultant Newtonian values are significantly lower than experimental values when UA model parameters regressed from equilibrium data are used. The Newtonian values were found to be very sensitive to the σ value used in the model. If Eq. (4) is used to obtain the σ values of the UA–CH_X groups, good agreement with experiment is obtained at all nine conditions studied with a K value that

Table VI. Simulated and Experimental Viscosity and *VI* for NAH

T (K)	ρ (kmol·m^{-3})	Exp.[a] (mPa·s)	Sim. (mPa·s)
313	2.161	7.48	5.17 (−31%)
373	2.053	2.02	1.54 (−21%)
		VI = 125	*VI* = 109 (−13%)

[a]Ref. 30.

increases σ for $-CH_3$ by only about 4.5% above that regressed from equilibrium experimental data. This rather small increase in σ substantially increases the simulated viscosity. Although this same value of K greatly improved the simulated viscosities of the larger molecule, NAH, it unfortunately does not bring them into agreement with experimental values. The results for these two fluids are consistent with previous studies that have suggested that the better UA models can be used to obtain accurate values of the viscosity pressure coefficient and *VI* or *VN*, but absolute viscosities will generally be underpredicted if σ values obtained from smaller molecules are applied to models for synthetic lubricants. It would seem that all-atom models or UA models with σ values based on the molecular size are required to provide more quantitative agreement with experimental viscosities.

ACKNOWLEDGMENT

Support of this project by Neste Oil Company, Espoo, Finland, is gratefully acknowledged.

REFERENCES

1. E. W. Dean and G. H. B. Davis, *Chem. & Met. Eng.* **36**:618 (1929).
2. ASTM D 2270-93, re-approved 1998.
3. E. W. Hardiman and A. H. Nissan, *J. Inst. Petr.* **31**:255 (1945).
4. M. P. Allen and D. J. Tildesley, *Computer Simulation of Liquids* (Clarendon, Oxford, 1987).
5. D. J. Evans and G. P. Morris, *Statistical Mechanics of Nonequilibrium Liquids* (Academic, London, 1990).
6. P. T. Cummings and D. J. Evans, *Ind. Eng. Chem. Res.* **31**:1237 (1992).
7. R. Edberg, G. P. Morriss, and D. J. Evans, *J. Chem. Phys.* **86**:4555 (1987).
8. A. Berker, S. Chynoweth, U. C. Clomp, and Y. Michopoulos, *J. Chem. Soc. Faraday Trans.* **88**:1719 (1992).
9. R. L. Rowley and J. F. Ely, *Molec. Phys.* **72**:831 (1991); **75**:713 (1992).
10. P. J. Daivis, D. J. Evans, and G. P. Morriss, *J. Chem. Phys.* **97**:616 (1992).
11. R. Khare, J. de Pablo, and A. Yethiraj, *J. Chem. Phys.* **107**:6956 (1997).
12. M. Lahtela, M. Linnolahti, T. A. Pakkanen, and R. L. Rowley, *J. Chem. Phys.* **108**:2626 (1998).
13. D. R. Wheeler and R. L. Rowley, *Molec. Phys.* **94**:555 (1998).
14. N. G. Fuller and R. L. Rowley, *Int. J. Thermophys.* **19**:1039 (1998).
15. Y. Yang, T. A. Pakkanen, and R. L. Rowley, *Int. J. Thermophys.* **21**:703 (2000).
16. J. D. Moore, S. T. Cui, P. T. Cummings, and H. D. Cochran, *AIChE J.* **43**:3260 (1997).
17. S. T. Cui, P. T. Cummings, H. D. Cochran, J. D. Moore, and S. A. Gupta, *Int. J. Thermophys.* **19**:449(1998).
18. L. I. Kioupis and E. J. Maginn, *J. Phys. Chem. B.* **103**:10781 (1999).
19. J. D. Moore, S. T. Cui, H. D. Cochran, and P. T. Cummings, *J. Chem. Phys.* **113**:8833 (2000).

20. C. McCabe, S. Cui, P. T. Cummings, P. A. Gordon, and R. B. Saeger, *J. Chem. Phys.* **114**:1887 (2001).
21. J. I. Siepmann, S. Karaborni, and B. Smit, *Nature* **365**:330 (1993).
22. M. J. Frisch, G. W. Trucks, and H. B. Schleget et al., *Gaussian 98*, Revision A.6 (Gaussian, Pittsburgh, PA, 1998).
23. M. Mondello and G. S. Grest, *J. Chem. Phys.* **103**:7156 (1995).
24. W. L. Jorgensen, J. D. Madura, and C. J. Swenson, *J. Am. Chem. Soc.* **106**:6638 (1984).
25. Y. Yang, *Application of Molecular Simulations to Synthetic Lubricant Research*, Ph.D. Dissertation (Brigham Young University, 2001).
26. D. J. Evans and G. P. Morriss, *Comput. Phys. Rep.* **1**:297 (1984).
27. R. Edberg, D. J. Evans, and G. P. Morriss, *J. Chem. Phys.* **84**:6933 (1986).
28. C. J. Mundy, M. L. Klein, and J. I. Siepmann, *J. Phys. Chem.* **101**:16779 (1996).
29. A. Et-Tahir, C. Boned, B. Lagourette, and P. Xans, *Int. J. Thermophys.* **16**:1309 (1995).
30. Private Communication with Neste Oil Co., Espoo, Finland.